Premigration data anti-aliasing for reverse time migration

Kawin Nimsaila*, Guangfu Shao, Rongxin Huang, and Ping Wang (CGG)

Summary

If the migration frequency is high (e.g., 50 Hz), reverse time migration (RTM) can be computationally very expensive and hardware demanding for large 3D data sets with large apertures. For this reason, while the vertical wave-propagation grid is chosen to be dense enough to hold the highest frequency content, a sparser than needed horizontal wave-propagation grid is often used to make high-frequency RTM affordable. As a result, the theoretically alias-free RTM operator suffers from aliasing issues when applied to high-frequency data with steep surface angles. To solve this aliasing issue, we propose first decomposing the input shot gathers of the common-shot RTM into the plane-wave domain using sparse inversion and then applying surface-angle-dependent anti-aliasing filters to individual plane-wave coefficients before transforming them back to the spatial domain. Using 2D synthetic and 3D field data examples, we demonstrate that our method allows RTM to migrate data with a frequency higher than the Nyquist frequency imposed by the horizontal wave-propagation grid without much suffering from aliasing problems.

Introduction

Aliasing in seismic processing can be broadly classified into three types: data aliasing, migration operator aliasing, and imaging aliasing. We focused on migration operator aliasing and data aliasing. Aliasing issues in a Kirchhoff migration operator can be solved either by interpolating input data to a denser grid or applying anti-aliasing filters during the migration (Gray, 1992; Lumley et al., 1994; Abma et al., 2005; Zhang et al., 2001).

RTM is performed in the frequency domain either explicitly (Larson, 1999) or implicitly (Zhang et al., 2007) and thus is alias-free when the wave-propagation grid in all three spatial directions is dense enough to hold the highest frequency content in the input data (Gray, 2013).

If the migration frequency is high (e.g., 50 Hz), RTM is computationally very expensive and hardware demanding for large 3D data sets with large apertures. To make high-frequency RTM affordable or possible at all, one commonly-adopted strategy is to use an uneven spatial grid in RTM wave propagation: the vertical grid is dense enough (e.g., <10 m) to hold the highest frequency content in the input data, whereas the horizontal grid is chosen to be coarser (e.g., 50 m × 50 m). By doing this, the computational cost and memory usage can be significantly reduced, and the majority of the high-frequency events with small surface angles can still be correctly propagated and migrated despite the sparse horizontal grid. However, high-frequency reflection data with steep surface angles will suffer from aliasing issues that degrade the RTM images. One solution is to apply angle-dependent anti-aliasing filters to input shot gathers in either the $f - k$ or $f - p$ domains. This requires an un-aliased estimation of the $f - k$ or $f - p$ coefficients of the input data. The sparse crossline sampling (e.g., 100/120 m) in towed-streamer acquisitions, however, makes this less straightforward. In this case, an algorithm that can handle strong spatial aliasing during plane-wave decomposition is required.

Wang and Nimsaila (2014) presented a progressive sparse Tau-P inversion scheme that works well for plane-wave decomposition in the presence of strong spatial aliasing. We propose using the same algorithm to decompose the input shot gathers into the plane-wave domain before applying surface-angle-dependent anti-aliasing filters to individual plane-wave coefficients and then transforming them back to the spatial domain.

Method

Progressive sparse Tau-P inversion has been proposed for plane-wave decomposition in the presence of strong spatial aliasing (Wang and Nimsaila, 2014). A sparse $f - p_x - p_y$ model, M, can be found to fit the input data, D, through a weighted inversion process:

$$D(f; x^i, y^i) = \sum_j e^{-i2\pi f(x^i p_x^j + y^i p_y^j)} M(f; p_x^j, p_y^j), \quad (1)$$

where f is frequency, (x^i, y^i) is the receiver location, and (p_x^j, p_y^j) is the slowness pair (i: trace index; j: slowness index). A fast Fourier transform (FFT) is applied to transform time, τ or t, into frequency, f.

With this $f - p_x - p_y$ model, we can compute the surface incidence angles (relative to the vertical direction), θ_x and θ_y, in x- and y-directions, respectively:

$$\begin{cases} \sin(\theta_x) = v_w |p_x^j| \\ \sin(\theta_y) = v_w |p_y^j| \end{cases} \quad (2)$$

Then, the maximum un-aliased frequency for common-shot RTM can be calculated based on the sampling theory if the horizontal wave-propagation grid, $(\Delta x, \Delta y)$, is given (vertical grid is assumed to be dense enough and thus is not considered):

$$f_{max} = \frac{v_w}{2\max(\Delta x \sin(\theta_x), \ \Delta y \sin(\theta_y))}. \quad (3)$$

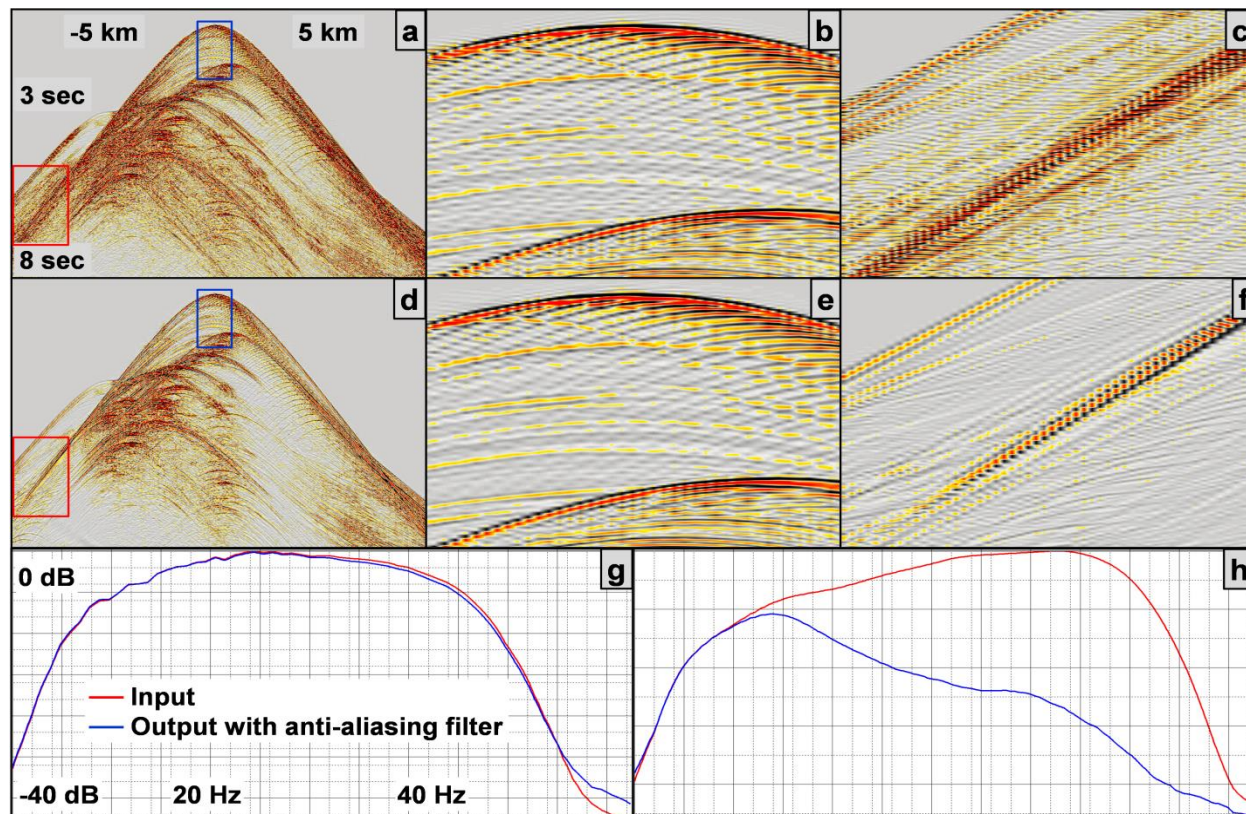Plugging Equation 2 into Equation 3 gives:

Figure 1: (a) Synthetic shot gather generated from the SEAM I model and (d) shot gather with premigration anti-aliasing. (b) and (e) are zoomed-in sections of the blue box in (a) and (d), respectively. (c) and (f) are zoomed-in sections of the red box in (a) and (d), respectively. Amplitude spectra of the blue and red boxes are displayed in (g) and (h), respectively.

$$f_{max} = \frac{1}{2\max(\Delta x |p_x^j|,\ \Delta y |p_y^j|)}. \tag{4}$$

Using the high-cut frequency computed from Equation 4, an angle-dependent anti-aliasing filter, $F(\Delta x, \Delta y; p_x^j, p_y^j)$, can be designed and applied to obtain the data after anti-aliasing:

$$D_a(f; x^i, y^i) =$$
$$\sum_j e^{-i2\pi f\left(x^i p_x^j + y^i p_y^j\right)} F(\Delta x, \Delta y; p_x^j, p_y^j) M(f; p_x^j, p_y^j). \tag{5}$$

Synthetic Data Examples

To demonstrate our anti-aliasing method, we first used 2D synthetic data modeled from the SEAM I model with a regular receiver spacing of 50 m. The data sampling interval was 8 ms; the frequency ranged from 0 to 60 Hz. The target horizontal migration grid was 50 m. Using Equation 4, we obtained a high-cut frequency of 15 Hz for a surface incidence angle of 90^0, and the angle corresponding to a high-cut frequency of 60 Hz was 14.5^o

(i.e., any events with surface incidence angles smaller than this value will not be affected by our anti-aliasing process).

Figure 1 compares a shot gather with and without the application of our premigration anti-aliasing process. Figures 1b and 1e show the zoomed-in sections around near channels before and after our anti-aliasing process. Both data sets look similar, and the amplitude spectra are similar as well (Figure 1g). The reason for this is that at the near offsets, the waves propagate mainly in the vertical direction, and thus the surface incidence angles are mostly smaller than 14.5^o. Therefore, the high-cut frequencies of our anti-aliasing filters are higher than 60 Hz for most events, and thus most energy is untouched by our anti-aliasing process.

On the contrary, there are significant differences between Figures 1c and 1f. This is because at large offsets, the surface angle was close to 90°; therefore, the high-cut frequency of the anti-aliasing filter was approximately 15 Hz. After our anti-aliasing process, the aliased energy in Figure 1c was largely removed (Figure 1f). There was a
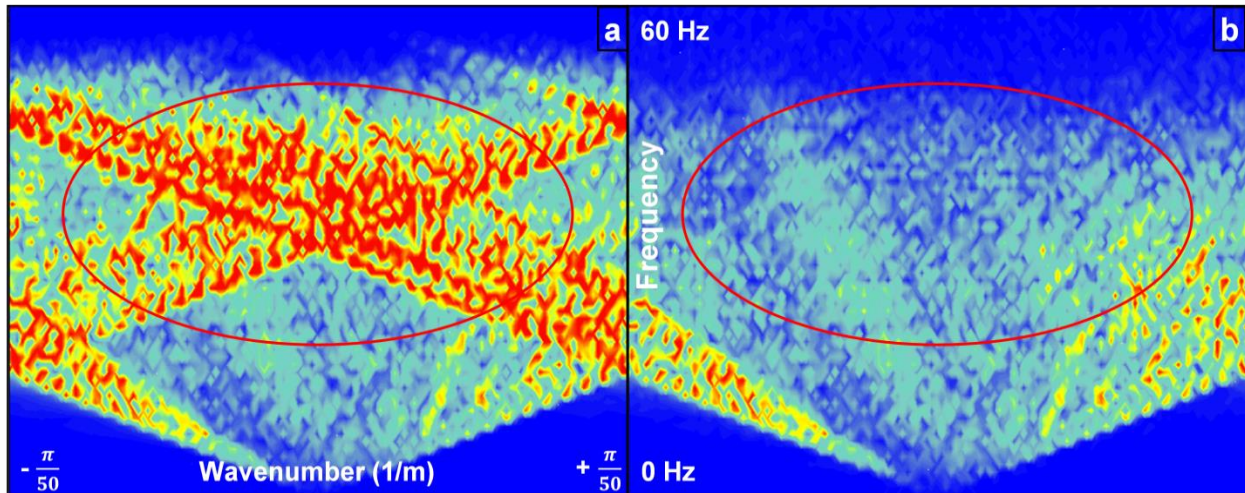
Premigration data anti-aliasing for RTM

Figure 2: Frequency-wavenumber, $f - k$, spectra of synthetic shots generated from the SEAM I model: (a) without premigration anti-aliasing; (b) with premigration anti-aliasing.

high frequency drop in the amplitude spectrum of the data after our anti-aliasing process (Figure 1h, blue line).

Figure 2 shows the frequency-wavenumber, $f - k$, spectra of the data, before and after our anti-aliasing process, calculated from the full shot gathers displayed in Figures 1a and 1d. The red circle in Figure 2a shows the aliased energy present in the input data, which corresponds to high-wavenumber events (large surface incidence angles) folded back onto the Fourier components of low wavenumbers due to spatial aliasing. When it is not removed from the input data prior to migration, this aliased energy becomes migration noise and swings that overlay with true seismic events.

Figure 3 shows stacked RTM images with a maximum migration frequency of 45 Hz before and after our premigration anti-aliasing process. The horizontal wave propagation grid was 50 m, which was insufficient to hold 45 Hz data for large surface incidence angles. Therefore, there were strong migration swings in both shallow (Figure 3a) and deep (Figure 3c) windows using input data without our anti-aliasing process. On the other hand, the images using input data after our anti-aliasing process were considerably cleaner (Figures 3b and 3d).

Field Data Examples

Next, we applied our approach to a 3D wide azimuth data set from the Keathley Canyon area, Gulf of Mexico. We implemented RTM with a maximum frequency of 35 Hz. The horizontal migration grid was 50 m $\times$ 60 m. Figure 4 shows RTM images using the input data with and without our premigration anti-aliasing process in shallow (Figures 4a and 4b) and deep sections (Figures 4c and 4d). Compared to RTM images using input data without

premigration anti-aliasing process, RTM images using input data after our anti-aliasing process were cleaner with more coherent reflection events and a higher signal-to-noise ratio.

The RTM images using input data with our anti-aliasing process were as sharp as those using input data without premigration anti-aliasing (and sometimes even sharper for places with less migration noise). This is because our anti-aliasing process only removed the aliased high-frequency energy at large surface incidence angles and kept most of the high-frequency events for RTM images.

Conclusions

We proposed a premigration data anti-aliasing method to apply surface-angle-dependent high-cut filters in the sparse Tau-P domain. This process allows us to run un-aliased high-frequency RTM without the need for a dense horizontal grid. Using both synthetic and field data, we demonstrated that our method effectively removes the aliased high-frequency events with large surface incidence angles prior to migration and hence improves the RTM images.

Although our anti-aliasing process removes only the aliased high-frequency events with large surface incidence angles, it may still harm the high-frequency content of some seismic events similarly to any other anti-aliasing filter.
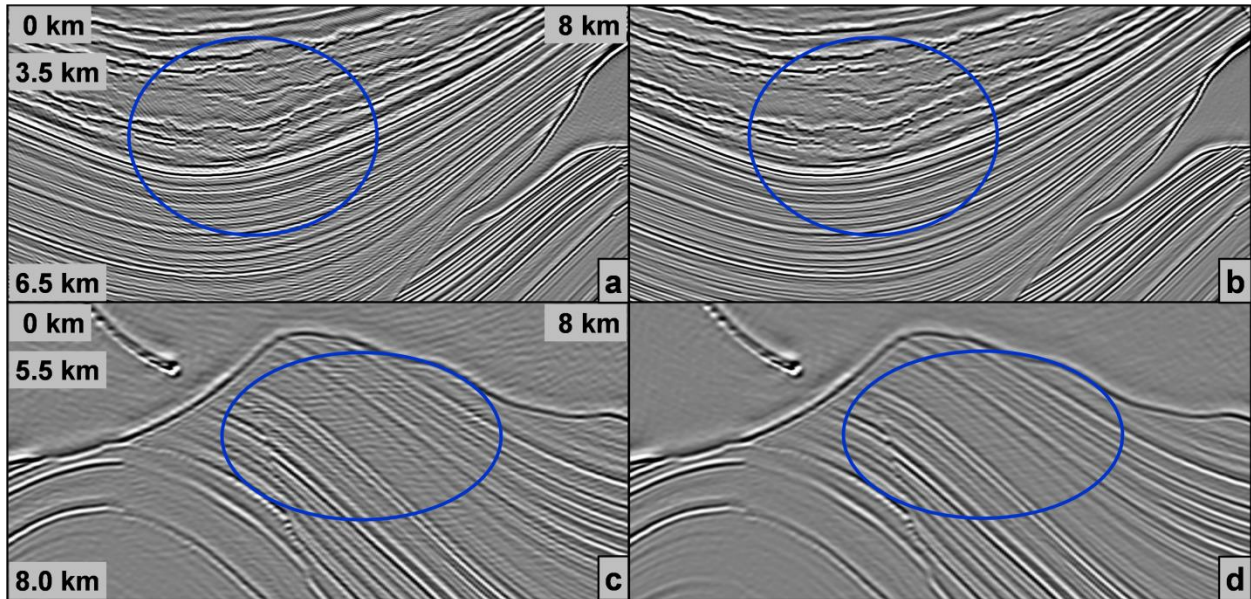
Acknowledgments

Figure 3: Reverse time migration (RTM) images of the shallow section using synthetic input data (a) without and (b) with premigration anti-aliasing. RTM images of subsalt section (c) without and (d) with premigration anti-aliasing.
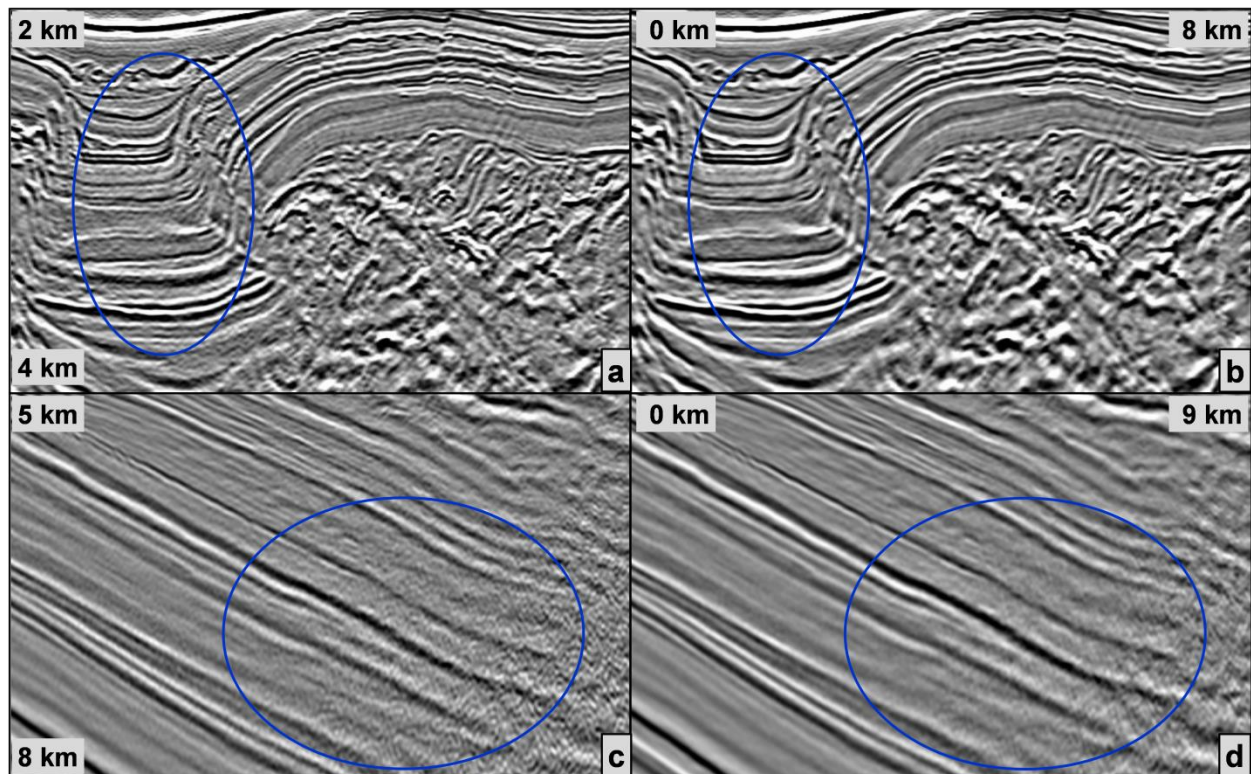

Figure 4: Reverse time migration (RTM) images of the shallow section using 3D WAZ input data (a) without and (b) with premigration anti-aliasing. RTM images of subsalt section (c) without and (d) with premigration anti-aliasing.

EDITED REFERENCES

Note: This reference list is a copyedited version of the reference list submitted by the author. Reference lists for the 2015 SEG Technical Program Expanded Abstracts have been copyedited so that references provided with the online metadata for each paper will achieve a high degree of linking to cited sources that appear on the Web.

REFERENCES

Abma, R., and N. Kabir, 2005, Comparison of interpolation methods: The Leading Edge, **24**, 984–989. http://dx.doi.org/10.1190/1.2112371.

Gray, S. H., 1992, Frequency-selective design of the Kirchhoff migration operator: Geophysical Prospecting, **40**, no. 5, 565–571. http://dx.doi.org/10.1111/j.1365-2478.1992.tb00541.x.

Gray, S. H., 2013, Spatial sampling, migration aliasing, and migrated amplitudes: Geophysics, **78**, no. 3, S157–S164. http://dx.doi.org/10.1190/geo2012-0451.1.

Larsson, E., 1999, A domain decomposition method for the Helmholtz equation in a multilayer domain: SIAM Journal on Scientific Computing, **20**, no. 5, 1713–1731. http://dx.doi.org/10.1137/S1064827597325323.

Lumley, D., J. Claerbout, and D. Bevc, 1994, Anti-aliased Kirchhoff 3-D migration: 64th Annual International Meeting, SEG, Expanded Abstracts, 1282–1285. http://dx.doi.org/10.1190/1.1822760.

Wang, P., and K. Nimsaila, 2014, Fast progressive sparse tau-p transform for regularization of spatially aliased seismic data: 84th Annual International Meeting, SEG, Expanded Abstracts, 3589–3593. http://dx.doi.org/10.1190/segam2014-0889.1.

Zhang, Y., S. H. Gray, J. Sun, and C. Notfors, 2001, Theory of migration anti-aliasing: 71st Annual International Meeting, SEG, Expanded Abstracts, 997–1000. http://dx.doi.org/10.1190/1.1816809.

Zhang, Y., J. Sun, and S. Gray, 2007, Reverse-time migration: amplitude and implementation issues: 77th Annual International Meeting, SEG, Expanded Abstracts, 2145–2149. http://dx.doi.org/10.1190/1.2792912.